

LC-TH-2000-033

DESY 00-003

UWThPh-2000-4

WUE-ITP-2000-005

HEPHY-PUB 727/2000

hep-ph/0004181

Beam Polarization and Spin Correlation Effects in Chargino Production and Decay ¹

G. MOORTGAT-PICK^{a2}, A. BARTL^{b3}, H. FRAAS^{c4}, W. MAJEROTTO^{d5}^a *DESY, Deutsches Elektronen-Synchrotron, D-22603 Hamburg, Germany*^b *Institut für Theoretische Physik, Universität Wien, A-1090 Wien, Austria*^c *Institut für Theoretische Physik, Universität Würzburg, D-97074 Würzburg, Germany*^d *Institut für Hochenergiephysik, Österreichische Akademie der Wissenschaften, A-1050 Wien, Austria*

Abstract

We study chargino production $e^+e^- \rightarrow \tilde{\chi}_1^+ \tilde{\chi}_1^-$ and the subsequent leptonic decay $\tilde{\chi}_1^- \rightarrow \tilde{\chi}_1^0 e^- \bar{\nu}_e$ including the complete spin correlations between production and decay. We work out the advantages of polarizing the e^+ and e^- beams. We study in detail the polarized cross sections, the angular distribution and the forward-backward asymmetry of the decay electron. They can be used to determine the sneutrino mass $m_{\tilde{\nu}_e}$.

¹Contribution to the Proceedings of the 2nd Joint ECFA/DESY study on Physics and Detectors for a Linear Electron-Positron Collider

²e-mail: gudrid@mail.desy.de

³e-mail: bartl@ap.univie.ac.at

⁴e-mail: fraas@physik.uni-wuerzburg.de

⁵e-mail: majer@hephy.oeaw.ac.at.

1 Introduction

If weak-scale supersymmetry (SUSY) is realized in nature, then SUSY particles will be observable at an e^+e^- linear collider with c.m.s. energy in the range $\sqrt{s} \leq 1$ TeV. The experimental study of charginos and the determination of their properties will be particularly important. The charginos $\tilde{\chi}_i^\pm$, $i = 1, 2$, are the mass eigenstates of the charged W-ino-higgsino system. In the Minimal Supersymmetric Standard Model (MSSM) their mass eigenvalues and eigenstates are determined by the parameters M_2 , μ and $\tan \beta$.

Previous papers mainly analyzed production cross sections and decay branching ratios in the MSSM (see, e.g. [1, 2] and references therein). Recently in [3] a method has been proposed for determining the SUSY parameters M_2 , μ , $\tan \beta$ and $m_{\tilde{\nu}_e}$ by measuring suitable observables in $e^+e^- \rightarrow \tilde{\chi}_i^+ \tilde{\chi}_j^-$, $i, j = 1, 2$. For a determination of the properties of charginos it is necessary to measure also angular distributions and angular correlations of the decay products. In the calculation of these observables the full spin correlations between chargino production and decay have to be taken into account. This has been done in recent analyses in [4, 5], where the process

$$e^+e^- \rightarrow \tilde{\chi}_i^+ \tilde{\chi}_j^- \quad (1)$$

with polarized beams and the subsequent leptonic decays

$$\tilde{\chi}_j^- \rightarrow \tilde{\chi}_k^0 \ell^- \bar{\nu}_\ell \quad (2)$$

have been studied. In [4] analytical formulae including the complete spin correlations have been presented. These formulae are also applicable in the case of complex couplings. The Feynman diagrams for the production (1) and the decay (2) are shown in Fig. 1.

The present paper is based on our analyses in [4, 6]. We study chargino production and decay with polarized e^+ and e^- beams. We use the MSSM as general framework and give predictions for the total cross section, the angular distribution of the decay lepton, and its forward-backward asymmetry. We show that using polarized e^+ beams together with polarized e^- beams can enhance the cross sections and can give additional information on the mixing character of the charginos and the masses of the exchanged particles. We study the $m_{\tilde{\nu}_e}$ and $m_{\tilde{e}_L}$ dependence of the decay lepton forward-backward asymmetry, which can be used to determine $m_{\tilde{\nu}_e}$.

2 Differential Cross Section

The differential cross section for the combined reaction of (1) and (2) is given by:

$$d\sigma_e = \frac{1}{2s} |T|^2 (2\pi)^4 \delta^4(p_1 + p_2 - \sum_i p_i) d\text{lips}(p_3 \dots p_{10}), \quad (3)$$

where $d\text{lips}(p_3 \dots p_{10})$ is the Lorentz invariant phase space element. The amplitude squared is [4]

$$\begin{aligned} |T|^2 = & 4|\Delta(\tilde{\chi}_i^+)|^2 |\Delta(\tilde{\chi}_j^-)|^2 \left(P(\tilde{\chi}_i^+ \tilde{\chi}_j^-) D(\tilde{\chi}_i^+) D(\tilde{\chi}_j^-) \right. \\ & + \sum_{a=1}^3 \Sigma_P^a(\tilde{\chi}_i^+) \Sigma_D^a(\tilde{\chi}_i^+) D(\tilde{\chi}_j^-) + \sum_{b=1}^3 \Sigma_P^b(\tilde{\chi}_j^-) \Sigma_D^b(\tilde{\chi}_j^-) D(\tilde{\chi}_i^+) \\ & \left. + \sum_{a,b=1}^3 \Sigma_P^{ab}(\tilde{\chi}_i^+ \tilde{\chi}_j^-) \Sigma_D^a(\tilde{\chi}_i^+) \Sigma_D^b(\tilde{\chi}_j^-) \right), \end{aligned} \quad (4)$$

where $P(\tilde{\chi}_i^+ \tilde{\chi}_j^-)$ ($D(\tilde{\chi}_i^+)$, $D(\tilde{\chi}_j^-)$) denotes the part of the unnormalized spin density matrix (decay matrix), which is independent of the chargino polarization, and $\Sigma_P^a(\tilde{\chi}_i^+)$, $\Sigma_P^b(\tilde{\chi}_j^-)$, $\Sigma_P^{ab}(\tilde{\chi}_i^+ \tilde{\chi}_j^-)$ ($\Sigma_D^a(\tilde{\chi}_i^+)$, $\Sigma_D^b(\tilde{\chi}_j^-)$) denote those parts of the spin density matrix (decay matrix) which depend on the chargino polarization. If all spin correlations are neglected, then only the first term contributes. The second and third term describe the spin correlations between production and decay. Σ_P^1 denotes the transverse polarization in the production plane, Σ_P^2 is the polarization perpendicular to the production plane, and Σ_P^3 is the longitudinal polarization of the decaying chargino. Σ_P^{ab} is due to the correlations between the polarizations of both decaying charginos, with $a, b = 1, 2$ referring to transverse chargino polarizations, and $a, b = 3$ referring to longitudinal polarization. The chargino propagators are given by $\Delta(\tilde{\chi}_k^\pm) = 1/[p_k^2 - m_k^2 + im_k\Gamma_k]$ with four-momentum p_k , mass m_k , and total width Γ_k of the decaying particle. For more details we refer to [4, 6, 7].

3 Numerical Analysis and Discussion

In the MSSM [8] the masses and couplings of charginos and neutralinos are functions of the parameters M_1 , M_2 , μ , $\tan\beta$, with M_1 normally fixed by the GUT relation $M_1 = \frac{5}{3}M_2 \tan^2\Theta_W$. As we do not consider CP violating effects, the parameters can be chosen real. The explicit expressions for the

neutralino and chargino mass mixing matrices can be found in [1] (note that in Refs. [1, 4, 6] the notation M' and M for M_1 and M_2 was used).

We will study a gaugino-like and a higgsino-like scenario, which we denote by A and B, respectively. Scenario A [9] is a mSUGRA scenario with the corresponding MSSM parameters given in Table 1. $\tilde{\chi}_1^\pm$ and $\tilde{\chi}_1^0$ have a large gaugino component. For easier comparison we want to have in the higgsino-like scenario B similar masses for $\tilde{\chi}_1^\pm$, $\tilde{\chi}_1^0$, $\tilde{\nu}_e$ and \tilde{e}_L . Therefore we have relaxed the GUT relation for the gaugino mass parameters. The parameters of scenario B are given in Table 1.

3.1 Beam polarization dependence of the total cross section

In Figs. 2a and b we show the cross section $\sigma(e^+e^- \rightarrow \tilde{\chi}_1^+ \tilde{\chi}_1^-)$ at $\sqrt{s} = 2m_{\tilde{\chi}_1^\pm} + 10$ GeV for scenarios A and B, respectively, as a function of the electron beam polarization P_-^3 and positron beam polarization P_+^3 (with $P_\pm^3 = \{-1, 0, 1\}$ for {left-,un-, right-} polarized). The white area is covered by an electron polarization $|P_-^3| \leq 85\%$ and a positron polarization $|P_+^3| \leq 60\%$. It can be seen that the beam polarizations may be used to enhance the cross section. One can gain a factor of about two by polarizing the positron beam in addition to the electron beam. Owing to the $\tilde{\nu}_e$ exchange the effect is biggest if the electron is left and the positron right polarized. We choose \sqrt{s} not too far from threshold, because the spin correlations to be discussed below decrease with \sqrt{s} [4].

Since in the chargino process the $\tilde{\nu}_e$ exchange in the t-channel favours left polarized electron beams and right polarized positron beams, one expects for gaugino-like scenarios the following sequence of polarized cross sections [10] for $|P_-^3| = 85\%$ and $|P_+^3| = 60\%$ (these values of $|P_-^3|$ and $|P_+^3|$ are used throughout the paper):

$$\sigma_e^{-+} > \sigma_e^{-0} > \sigma_e^{00} > \sigma_e^{--} > \sigma_e^{++} > \sigma_e^{+0} > \sigma_e^{+-}. \quad (5)$$

Here $(-+)$ etc. denotes the sign of the electron polarization P_-^3 and of the positron polarization P_+^3 , respectively, and σ_e is defined as

$$\sigma_e = \sigma(e^+e^- \rightarrow \tilde{\chi}_1^+ \tilde{\chi}_1^-) \times BR(\tilde{\chi}_1^- \rightarrow \tilde{\chi}_1^0 e^- \bar{\nu}_e), \quad (6)$$

where we assume that only one chargino decays leptonically.

For pure higgsinos near threshold one would have due to Z^0 exchange

$$\sigma_e^{-+} > \sigma_e^{+-} > \sigma_e^{-0} > \sigma_e^{00} > \sigma_e^{+0} > \sigma_e^{--} > \sigma_e^{++}. \quad (7)$$

Since in chargino pair production also γ exchange contributes, the relations (5), (7) are only approximately valid. Nevertheless, one can get additional

information if the electron and the positron beam are polarized, since the sequences of polarized cross sections for gaugino-like and higgsino-like scenarios are different. If one had only the electron beam polarized, in both scenarios one would obtain the same sequence of polarized cross sections, namely $\sigma^{-0} > \sigma^{00} > \sigma^{+0}$.

In scenario A we get for $|P_-^3| = 85\%$ and $|P_+^3| = 60\%$ at $\sqrt{s} = 2m_{\tilde{\chi}_1^\pm} + 10$ GeV the results given in Table 2. They fulfil the relation (5) for polarized cross sections. However, in the higgsino-like scenario B the sequence is different from relation (7) due to γ exchange and in particular γZ^0 interference.

3.2 Spin effects in the lepton angular distribution and in the lepton forward-backward asymmetry

We will discuss the lepton angular distribution $d\sigma_e/d\cos\Theta_e$ in the overall c.m.s. of the combined reactions (1) and (2). Here Θ_e denotes the angle between the electron beam and the outgoing e^- . The forward-backward asymmetry A_{FB} of the decay lepton is defined as

$$A_{FB} = \frac{\sigma_e(\cos\Theta_e > 0) - \sigma_e(\cos\Theta_e < 0)}{\sigma_e(\cos\Theta_e > 0) + \sigma_e(\cos\Theta_e < 0)}. \quad (8)$$

This observable is very sensitive to the gaugino component of the chargino and the mass of the exchanged sneutrino and slepton. While in σ_e , eq. (6), the leptonic branching ratio of $\tilde{\chi}_1^-$ enters, which depends on the parameters of the squark sector, A_{FB} , eq. (8), has the advantage of being independent of the squark sector.

First we discuss how the spin correlations depend on the mixing character of the charginos [4]. In Figs. 3a and b we show the angular distribution $d\sigma_e/d\cos\Theta_e$ of the decay lepton for scenarios A and B, respectively, for unpolarized beams and for both beams polarized at $\sqrt{s} = 2m_{\tilde{\chi}_1^\pm} + 10$ GeV. The angular distributions are compared with those, where no spin correlations are taken into account. Without spin correlations the $\cos\Theta_e$ dependence would be much flatter. It can also be seen that the spin correlations are more important in the gaugino-like scenario.

In Figs. 4a and b A_{FB} is shown with and without spin correlations as a function of \sqrt{s} for the two scenarios. In the gaugino-like scenario A A_{FB} can reach 40% at $\sqrt{s} = 500$ GeV. The large asymmetry in scenario A, Fig. 4a, is due to the $\tilde{\nu}_e$ exchange in the crossed channel. Also the \tilde{e}_L exchange in the decay $\tilde{\chi}_1^- \rightarrow \tilde{\chi}_1^0 e^- \tilde{\nu}_e$ plays an important role. Therefore in the gaugino-like scenario A A_{FB} depends appreciably on $m_{\tilde{e}_L}$ (see also Fig. 7).

In the higgsino-like scenario, Fig. 4b, Z^0 and W^\pm exchanges in production and decay, respectively, dominate. Therefore, A_{FB} is much smaller, $A_{FB} \leq 8\%$. However, in both scenarios, close to threshold, A_{FB} would be one order of magnitude smaller if the spin correlations are neglected. For fixed chargino masses the correlations decrease with \sqrt{s} . This happens more rapidly in the gaugino case. At energies far from the threshold the charginos have a large energy, and the decay lepton has essentially the same direction as the chargino [11].

In scenario A the dependence of A_{FB} on the polarizations of the beams is very weak, see Table 2. The enhancement of the cross section for left polarized electron beams and for right polarized positron beams is cancelled in the ratio of the cross sections $\sigma_e(\cos\Theta_e)$ in (8). In scenario B A_{FB} depends more strongly on the polarizations of the beams, see Table 2. The Z^0 couplings to the higgsino components of the charginos determine the behaviour of A_{FB} . The sign of A_{FB} can even flip if the polarization of the electron beam is changed from left to right due to the dominating axial coupling of $Z^0 e^+ e^-$. However, since the crossed channel contributions are suppressed, A_{FB} is smaller than in scenario A and lies between -6% and $+8\%$.

3.3 Sneutrino mass dependence of σ_e and A_{FB}

If the chargino $\tilde{\chi}_1^\pm$ has a substantial gaugino component, the sneutrino exchange in the t-channel has a strong influence on the cross section and angular distribution of chargino production. In [12, 13] it was studied if the sneutrino mass $m_{\tilde{\nu}_e}$ can be determined from the angular distribution of the production process $e^+ e^- \rightarrow \tilde{\chi}_1^+ \tilde{\chi}_1^-$. In this subsection we study the $m_{\tilde{\nu}_e}$ dependence of the cross section σ_e , eq. (6), as well as the decay lepton angular distribution of $e^+ e^- \rightarrow \tilde{\chi}_1^+ \tilde{\chi}_1^-$, $\tilde{\chi}_1^- \rightarrow \tilde{\chi}_1^0 e^- \tilde{\nu}_e$, and the decay lepton forward-backward asymmetry A_{FB} , eq. (8). As these observables depend decisively on the spin correlations, it is instructive to have a closer look on their $m_{\tilde{\nu}_e}$ dependence. These observables also depend on the slepton mass $m_{\tilde{e}_L}$, due to the \tilde{e}_L exchange in the decay amplitude. Since $\tilde{\ell}_L$ and $\tilde{\nu}_\ell$ are members of the same $SU(2)_L$ doublet, we assume the relation [13, 14]

$$m_{\tilde{\ell}_L}^2 = m_{\tilde{\nu}_\ell}^2 - m_W^2 \cos 2\beta \quad (9)$$

between their masses, with m_W the mass of the W^\pm boson. As this relation is based on weak $SU(2)_L$ symmetry, it has to be fulfilled at tree level, and can only be modified by radiative corrections.

	M_1	M_2	μ	$\tan\beta$	$m_{\tilde{e}_L}$	$m_{\tilde{\nu}_e}$	$m_{\tilde{\chi}_1^\pm}$	$m_{\tilde{\chi}_2^\pm}$	$m_{\tilde{\chi}_1^0}$	$m_{\tilde{\chi}_2^0}$	$\Gamma_{\tilde{\chi}_1^\pm}$
A	78	152	316	3	176	161	128	357	71	130	84E-6
B	95	400	145	3	176	161	129	421	71	149	217E-6

Table 1: SUSY parameters and masses in scenarios A [9] and B. Masses and total width are given in GeV.

	$\sqrt{s} = 2m_{\tilde{\chi}_1^\pm} + 10 \text{ GeV}$						
A	(-+)	(-0)	(00)	(--)	(++)	(+0)	(+-)
σ_e/fb	59	37	20	15	5	3	1
$A_{FB}/\%$	33	33	33	33	32	31	25
B	(-+)	(-0)	(00)	(--)	(+-)	(+0)	(++)
σ_e/fb	152	96	59	40	26	22	18
$A_{FB}/\%$	8	8	6	7	-6	-3	3

Table 2: Polarized cross sections $\sigma_e = \sigma(e^+e^- \rightarrow \tilde{\chi}_1^+ \tilde{\chi}_1^-) \times BR(\tilde{\chi}_1^- \rightarrow \tilde{\chi}_1^0 e^- \nu_e)/\text{fb}$ and forward-backward asymmetries A_{FB} of the decay electron at $\sqrt{s} = 2m_{\tilde{\chi}_1^\pm} + 10 \text{ GeV}$ in scenarios A and B, see Table 1, for unpolarized beams (00), only electron beam polarized (-0), (+0) with $P_-^3 = \pm 85\%$ and both beams polarized with $P_-^3 = \pm 85\%$, $P_+^3 = \pm 60\%$.

In Figs. 5a and b we show σ_e as a function of $m_{\tilde{\nu}_e}$ for three sets of e^- and e^+ beam polarizations $(P_-^3, P_+^3) = (-85\%, +60\%), (-85\%, 0), (0, 0)$ at $\sqrt{s} = 2m_{\tilde{\chi}_1^\pm} + 10 \text{ GeV}$ and $\sqrt{s} = 500 \text{ GeV}$, respectively. The other SUSY parameters, apart from $m_{\tilde{\nu}_e}$ and $m_{\tilde{e}_L}$, are as in scenario A (Table 1). The cross section σ_e , as shown in Fig. 5a and b, exhibits a pronounced minimum, which is due to the destructive interference between Z exchange and $\tilde{\nu}_e$ exchange. For \sqrt{s} near threshold this minimum is approximately at $m_{\tilde{\nu}_e} \approx m_{\tilde{\chi}_1^\pm}$ and in the limit $\sqrt{s} \rightarrow 2m_{\tilde{\chi}_1^\pm}$ the minimum reaches exactly $m_{\tilde{\nu}_e} \rightarrow m_{\tilde{\chi}_1^\pm}$. For $\sqrt{s} = 500 \text{ GeV}$ the minimum is shifted to $m_{\tilde{\nu}_e} \approx 250 \text{ GeV}$ (Fig. 5b). Due to this minimum one gets an ambiguity when determining $m_{\tilde{\nu}_e}$ by measuring σ_e .

The cross section is biggest for left-polarized e^- beam and right-polarized e^+ beam. Compared to the unpolarized cross section one can gain a factor of 1.8 if only the e^- beam is polarized ($P_-^3 = -85\%$), and a factor of about 3 if both beams are polarized ($P_-^3 = -85\%, P_+^3 = +60\%$). Also the $m_{\tilde{\nu}_e}$ dependence is strongest for $(P_-^3, P_+^3) = (-, +)$. For $m_{\tilde{\nu}_e} \leq m_{\tilde{\chi}_1^\pm}$ the two-body decay $\tilde{\chi}_1^- \rightarrow e^- \tilde{\nu}_e$ is opening.

Also the decay lepton angular distribution depends significantly on $m_{\tilde{\nu}_e}$. In Figs. 6a and b we plot the $\cos \Theta_e$ distribution at $\sqrt{s} = 2m_{\tilde{\chi}_1^\pm} + 10$ GeV, for unpolarized and polarized beams, taking $m_{\tilde{\nu}_e} = 130$ GeV and 250 GeV, respectively. For $m_{\tilde{\nu}_e} = 130$ GeV (Fig. 6a) the $\cos \Theta_e$ distribution is relatively flat due to interference effects in the spin terms. In Fig. 6a, the $\cos \Theta_e$ distribution is a superposition of Z exchange and $\tilde{\nu}_e$ exchange behaviour. For $m_{\tilde{\nu}_e} = 250$ GeV (Fig. 6b) the $\cos \Theta_e$ distribution is mainly due to $\tilde{\nu}_e$ exchange and therefore has its maximum in the forward direction.

In Figs. 7a and b we show the decay lepton forward–backward asymmetry A_{FB} as a function of $m_{\tilde{\nu}_e}$ for polarized beams at $\sqrt{s} = 2m_{\tilde{\chi}_1^\pm} + 10$ GeV and $\sqrt{s} = 500$ GeV, respectively. In order to study the influence of $m_{\tilde{e}_L}$ on the decay, we calculate A_{FB} for $m_{\tilde{e}_L} = 130$ GeV, 150 GeV, 200 GeV, and for $m_{\tilde{e}_L}$ fulfilling relation (9). The other SUSY parameters are as in scenario A (Table 1). The minimum of A_{FB} is due to spin correlations. For $\sqrt{s} = 2m_{\tilde{\chi}_1^\pm} + 10$ GeV ($\sqrt{s} = 500$ GeV) A_{FB} depends quite sensitively on $m_{\tilde{\nu}_e}$ up to $m_{\tilde{\nu}_e} \approx 300$ GeV ($m_{\tilde{\nu}_e} \approx 1$ TeV). The decrease of A_{FB} for $m_{\tilde{\nu}_e} \gtrsim 200$ GeV ($m_{\tilde{\nu}_e} \gtrsim 300$ GeV) in Fig. 7a (Fig. 7b) is due to the decreasing $\tilde{\nu}_e$ exchange contribution for increasing $m_{\tilde{\nu}_e}$. For $\sqrt{s} = 2m_{\tilde{\chi}_1^\pm} + 10$ GeV and $m_{\tilde{\nu}_e} > 200$ GeV A_{FB} exhibits also an appreciable $m_{\tilde{e}_L}$ dependence for $m_{\tilde{e}_L} \leq 200$ GeV. Since the \tilde{e}_L exchange contributes only to the decay the dependence of A_{FB} on $m_{\tilde{e}_L}$ is weaker for $\sqrt{s} = 500$ GeV (Fig. 7b) than near threshold.

Turning now to the question whether the sneutrino mass $m_{\tilde{\nu}_e}$ can be determined from chargino pair production and decay, we first consider the case that $m_{\tilde{\nu}_e} \gtrsim \sqrt{s}/2$, where $\tilde{\nu}_e \tilde{\nu}_e$ pair production is kinematically not possible. At $\sqrt{s} = 500$ GeV the lepton forward–backward asymmetry A_{FB} , as shown in Fig. 7b, is sensitive to $m_{\tilde{\nu}_e}$. We will estimate the precision which can be expected if $m_{\tilde{\nu}_e}$ is determined from this observable. We assume that the slepton mass $m_{\tilde{e}_L}$ and the other SUSY parameters are known with good precision. For definiteness we take, e. g., $m_{\tilde{e}_L} = 200$ GeV, and the other SUSY parameters as in scenario A. If we take only the statistical error $\delta(A_{FB})$ and a luminosity of $\mathcal{L} = 500 \text{ fb}^{-1}$, A_{FB} can be measured up to $< \pm 1\%$. From Fig. 7b we can estimate that in the range $350 \text{ GeV} \lesssim m_{\tilde{\nu}_e} \lesssim 800 \text{ GeV}$ an error of about $\delta m_{\tilde{\nu}_e} < \pm 10 \text{ GeV}$ may be achieved. The experimental errors of $m_{\tilde{e}_L}$ and the other SUSY parameters are neglected. The ambiguity for $\sqrt{s} = 500$ GeV (Fig. 7b) in the range $250 \text{ GeV} \lesssim m_{\tilde{\nu}_e} \lesssim 350 \text{ GeV}$ can most probably be resolved by measuring A_{FB} at different c.m.s. energies. Similarly, at $\sqrt{s} = 2m_{\tilde{\chi}_1^\pm} + 10$ GeV (Fig. 7a), A_{FB} is quite sensitive to $m_{\tilde{\nu}_e}$ in the range $130 \text{ GeV} \lesssim m_{\tilde{\nu}_e} \lesssim 350 \text{ GeV}$ where direct production is not possible.

The ambiguity present in this $m_{\tilde{\nu}_e}$ range does not occur in σ_e . Hence, it can be resolved by using the data on A_{FB} and on σ_e . For a more quantitative assessment of the accuracy of $m_{\tilde{\nu}_e}$ that can be expected from measuring the decay lepton forward–backward asymmetry in chargino production, Monte Carlo studies taking into account experimental cuts and detector simulation would be necessary.

In case $m_{\tilde{\nu}_e} < \sqrt{s}/2$, $\tilde{\nu}_e\bar{\tilde{\nu}}_e$ pairs can be directly produced. If $m_{\tilde{\chi}_1^\pm} < m_{\tilde{\nu}_e} < \sqrt{s}/2$, then the visible decay $\tilde{\nu}_e \rightarrow e^- \tilde{\chi}_1^+$ is kinematically allowed, and will presumably have a sufficiently high branching ratio. We do not treat this case here, because measuring the cross section of $e^+e^- \rightarrow \tilde{\nu}_e\bar{\tilde{\nu}}_e$ at threshold will then allow us to determine $m_{\tilde{\nu}_e}$ with good accuracy [15]. If $m_{\tilde{\nu}_e} < m_{\tilde{\chi}_1^\pm} < \sqrt{s}/2$, then $\tilde{\nu}_e$ has no visible decay with sufficiently high branching ratio. However, the two-body chargino decay $\tilde{\chi}_1^- \rightarrow e^- \bar{\tilde{\nu}}_e$ is possible. Measuring the endpoints of the energy spectrum of the decay leptons e^+ and e^- will provide a very precise determination of the masses $m_{\tilde{\chi}_1^\pm}$ and $m_{\tilde{\nu}_e}$. The alternative method to determine $m_{\tilde{\nu}_e}$ by measuring the decay lepton forward–backward asymmetry A_{FB} of chargino production will, in principle, also be possible. However, the accuracy of $m_{\tilde{\nu}_e}$ obtainable in this way is expected to be lower than that from the decay lepton energy spectrum.

4 Conclusions

We have studied chargino production with both the e^- and e^+ beam polarized. By an appropriate choice of the polarization of both beams one can obtain up to three times larger cross sections. Also the sensitivity to the mixing character of the charginos and to the sneutrino mass is considerably enhanced. By taking into account the spin correlations between production and decay, we have investigated the angular distribution and the forward–backward asymmetry of the decay lepton of one of the charginos in $e^+e^- \rightarrow \tilde{\chi}_1^+ \tilde{\chi}_1^-$, $\tilde{\chi}_1^- \rightarrow \tilde{\chi}_1^0 e^- \bar{\nu}_e$. The forward–backward asymmetry strongly depends on the mixing character of the charginos.

We have studied in detail the dependence on $m_{\tilde{\nu}_e}$. For appropriate beam polarizations the cross section is particularly sensitive to $m_{\tilde{\nu}_e}$. Measuring the angular distribution and the forward–backward asymmetry will be useful for determining $m_{\tilde{\nu}_e}$ and thereby the mass relation $m_{\tilde{\ell}_L}^2 = m_{\tilde{\nu}_\ell}^2 - m_W^2 \cos 2\beta$ can be tested.

Acknowledgements

We would like to thank U. Martyn for very valuable discussions. We are grateful to W. Porod and S. Hesselbach for providing the computer programs for neutralino widths. This work was also supported by the German Federal Ministry for Research and Technology (BMBF) under contract number 05 7WZ91P (0), by the Deutsche Forschungsgemeinschaft under contract Fr 1064/2-2, and the ‘Fonds zur Förderung der wissenschaftlichen Forschung’ of Austria, Project No. P13139-PHY.

References

- [1] A. Bartl, H. Fraas, W. Majerotto, Z.Phys. **C 30** (1986) 441; A. Bartl, H. Fraas, W. Majerotto, B. Mößlacher, Z.Phys. **C 55** (1992) 257; A. Bartl, W. Majerotto, B. Mößlacher, in ‘ e^+e^- Collisions at 500 GeV: The Physics Potential’, Part B, DESY 92-123B, p. 641, ed. by P.M. Zerwas.
- [2] M. Chen, C. Dionisi, M. Martinez, X. Tata, Phys.Rep. **159** (1988) 201; S. Ambrosanio et al., in *Physics at LEP2*, CERN 96-01, Vol. 1, p. 463, eds. G. Altarelli, T. Sjöstrand and F. Zwirner; E. Accomando et al., Phys. Rep. **299** (1998) 1.
- [3] S.Y. Choi, A. Djouadi, H. Dreiner, J. Kalinowski, P. Zerwas, Eur. Phys. J. **C 7**, 123 (1999); S.Y. Choi, A. Djouadi, H.S. Song, P. Zerwas, Eur. Phys. J. **C 8**, 669 (1999); S.Y. Choi, M. Guchait, J. Kalinowski, P.M. Zerwas, hep-ph/0001175; S.Y. Choi, A. Djouadi, M. Guchait, J. Kalinowski, H.S. Song, P.M. Zerwas, hep-ph/0002033.
- [4] G. Moortgat-Pick, H. Fraas, A. Bartl, W. Majerotto, Eur. Phys. J. **C 7** (1999) 113.
- [5] V. Lafage et al., Int. J. Mod. Phys. **A14** (1999) 5075.
- [6] G. Moortgat-Pick, H. Fraas, Acta Phys.Polon. **B30** (1999) 1999.
- [7] G. Moortgat-Pick, A. Bartl, H. Fraas, W. Majerotto, hep-ph/0002253.
- [8] H.E. Haber, G.L. Kane, Phys. Rep. **117** (1985) 75.
- [9] S. Ambrosanio, G.A. Blair, P. Zerwas, ECFA-DESY LC-Workshop, 1998, <http://www.desy.de/conferences/ecfa-desy-lc98.html>.
- [10] G. Moortgat-Pick, PhD Thesis, Würzburg 1999.
- [11] J.L. Feng, M.J. Strassler, Phys. Rev. **D 55** (1997) 1326.

- [12] J. L. Feng, M. E. Peskin, H. Murayama, X. Tata, Phys. Rev. D 52 (1995) 1418.
- [13] T. Tsukamoto, K. Fujii, H. Murayama, M. Yamaguchi, Y. Okada, Phys. Rev. D **51** (1995) 3153.
- [14] S.P. Martin, P. Ramond, Phys. Rev. D **48** (1993) 5365.
- [15] U. Martyn, G. Blair, hep-ph/9910416, to be published in the Proceedings of 4th International Workshop on Linear Colliders (LCWS 99), Sitges, Barcelona, Spain, 28 April - 5 May 1999.

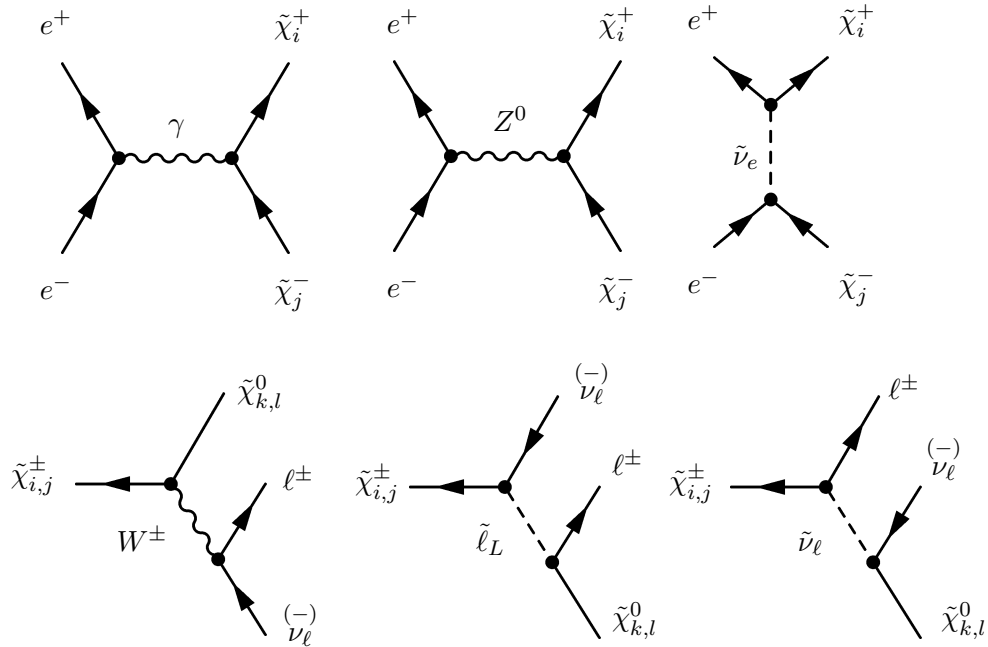


Figure 1: Feynman diagrams for the production $e^+ e^- \rightarrow \tilde{\chi}_i^+ \tilde{\chi}_j^-$ and the decay processes $\tilde{\chi}_{i,j}^\pm \rightarrow \tilde{\chi}_{k,l}^0 \ell^\pm \tilde{\nu}_\ell^{(-)}$.

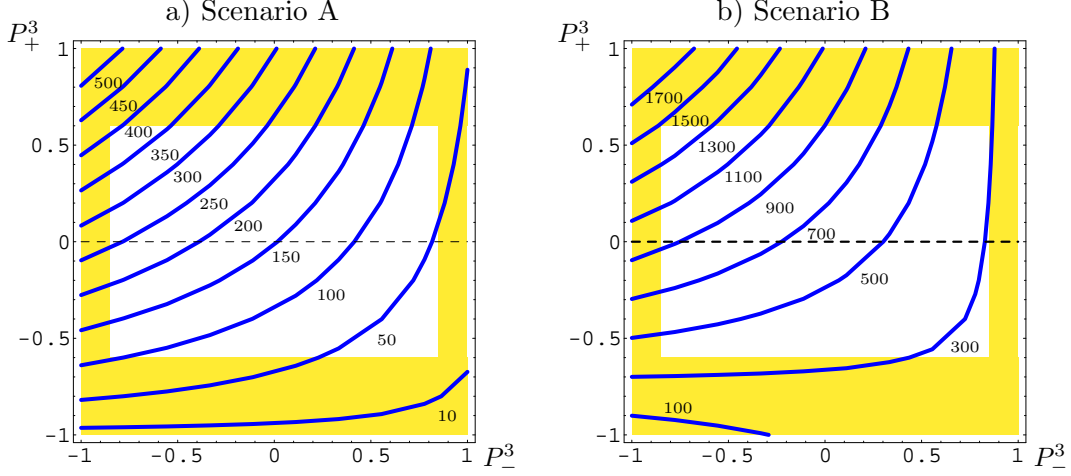


Figure 2: Contour lines of cross sections $\sigma(e^+e^- \rightarrow \tilde{\chi}_1^+ \tilde{\chi}_1^-)$ at $\sqrt{s} = 2m_{\tilde{\chi}_1^\pm} + 10$ GeV in a) scenario A and b) scenario B. The longitudinal beam polarization for electrons (positrons) is denoted by P_-^3 (P_+^3). The white region is for $|P_-^3| \leq 85\%$, $|P_+^3| \leq 60\%$ (dashed line if only the electron beam is polarized).

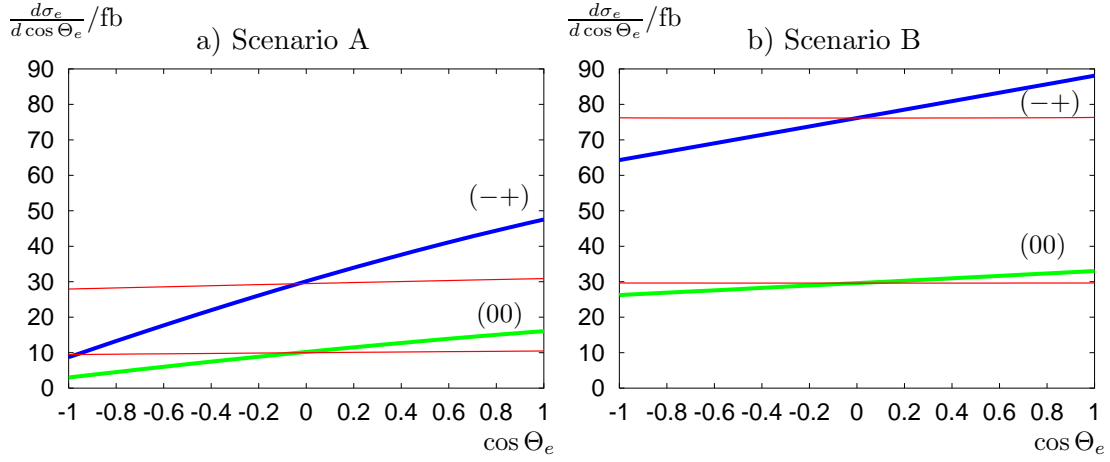


Figure 3: Lepton decay angular distribution at $\sqrt{s} = 2m_{\tilde{\chi}_1^\pm} + 10$ GeV in a) scenario A and b) scenario B with (thick lines) and without spin correlations (thin lines) for unpolarized beams (00) and for $P_- = -85\%$, $P_+ = +60\%$ $(-+)$, respectively.

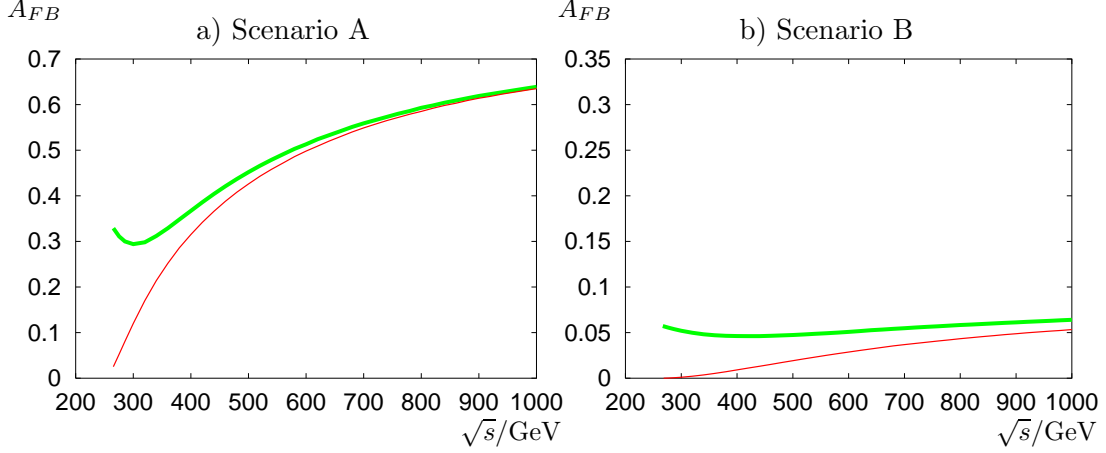


Figure 4: Forward-backward asymmetries of the decay electron $A_{FB}(e^+e^- \rightarrow \tilde{\chi}_1^+ \tilde{\chi}_1^-, \tilde{\chi}_1^- \rightarrow \tilde{\chi}_1^0 e^- \tilde{\nu}_e)/\%$ with (thick lines) and without spin correlations (thin lines) in a) scenario A and b) scenario B as a function of \sqrt{s} for unpolarized beams.

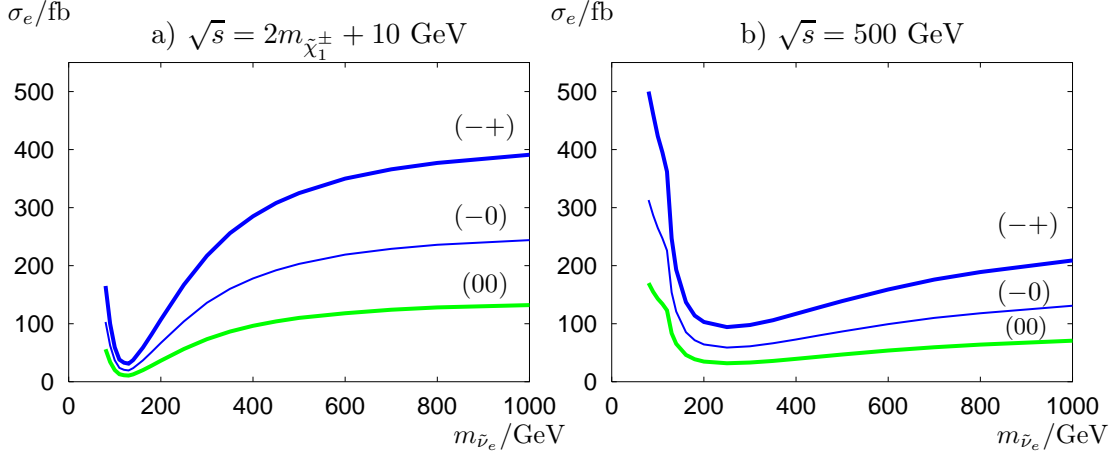


Figure 5: Cross Section $\sigma_e = \sigma(e^+e^- \rightarrow \tilde{\chi}_1^+ \tilde{\chi}_1^-) \times BR(\tilde{\chi}_1^- \rightarrow \tilde{\chi}_1^0 e^- \tilde{\nu}_e)$ in a) at $\sqrt{s} = 2m_{\tilde{\chi}_1^\pm} + 10$ GeV and in b) at $\sqrt{s} = 500$ GeV as function of $m_{\tilde{\nu}_e}$ for unpolarized beams (00), only the electron beam polarized $P_-^3 = -85\%$ (-0) and both beams polarized $P_-^3 = -85\%$, $P_+^3 = +60\%$ $(-+)$. Other parameters as in scenario A.

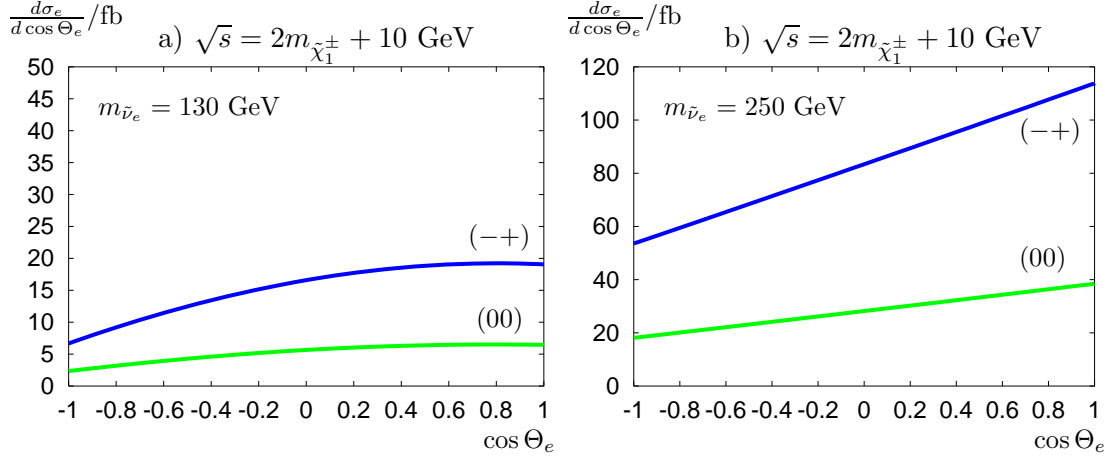


Figure 6: Lepton decay angular distribution at $\sqrt{s} = 2m_{\tilde{\chi}_1^\pm} + 10$ GeV for a) $m_{\tilde{\nu}_e} = 130$ GeV and b) $m_{\tilde{\nu}_e} = 250$ GeV for unpolarized beams (00) and for $P_- = -85\%$, $P_+ = +60\%$ $(-+)$. The other parameters as in scenario A but $m_{\tilde{e}_L}^2 = m_{\tilde{\nu}_e}^2 - m_W^2 \cos 2\beta$.

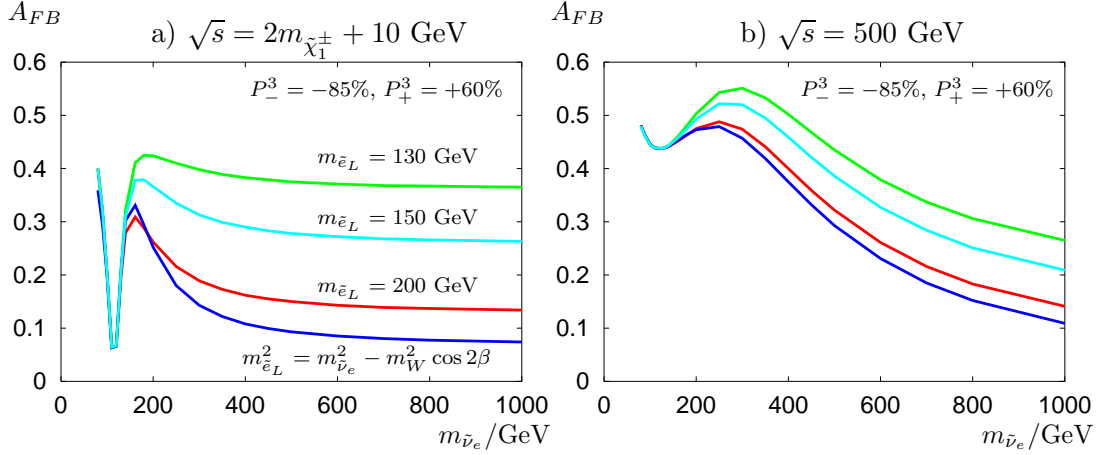


Figure 7: Forward-backward asymmetry of the decay electron $A_{FB}(e^+e^- \rightarrow \tilde{\chi}_1^+ \tilde{\chi}_1^-, \tilde{\chi}_1^- \rightarrow \tilde{\chi}_1^0 e^- \tilde{\nu}_e)/\%$ in a) at $\sqrt{s} = 2m_{\tilde{\chi}_1^\pm} + 10$ GeV and in b) $\sqrt{s} = 500$ GeV as function of $m_{\tilde{\nu}_e}$ for $m_{\tilde{e}_L} = 130$ GeV, $m_{\tilde{e}_L} = 150$ GeV, $m_{\tilde{e}_L} = 200$ GeV and $m_{\tilde{e}_L}$ fulfilling (9), for both beams polarized $P_-^3 = -85\%$, $P_+^3 = +60\%$ $(-+)$. Other parameters as in scenario A.